Evolution and future of the Lusi mud eruption inferred from ground deformation

M. L. Rudolph[1], M. Shirzaei[1], M. Manga[1], and Y. Fukushima[2]

The ongoing eruption of the Lusi mud volcano in East Java, Indonesia offers the unprecedented opportunity to study a large eruption from its beginning to its eventual end. We use new observations of ground deformation obtained from multitemporal interferometric analysis of L-band synthetic aperture radar data to show that Lusi will stop erupting much sooner than previously anticipated. Using principal component analysis, we find that the rate of ground deformation, and by implication, pressure in the mud source region, has been decaying exponentially with an e-folding time scale of 2.1 ± 0.4 years. We anticipate that discharge will decrease to 10% of the present rate in 5 years.

1. Introduction

The ongoing eruption of the Lusi mud volcano, East Java, Indonesia (Figure 1) offers the unprecedented opportunity to study a large eruption from its beginning to its eventual end. This eruption has devastated local communities, displacing more than 60,000 people and causing >$4B in economic losses [*Richards*, 2011]. Despite significant efforts to understand the eruption and predict its longevity [*Istadi et al.*, 2009; *Davies et al.*, 2011; *Rudolph et al.*, 2011; *Mazzini et al.*, 2012], the spatiotemporal evolution of the source feeding the eruption is not well understood.

We present new observations of ground deformation that indicate that Lusi will stop erupting much sooner than previously anticipated [*Istadi et al.*, 2009; *Davies et al.*, 2011; *Rudolph et al.*, 2011]. Previous assessments of the hazard posed by Lusi relied upon estimates of discharge during the first three years of the eruption [*Mazzini et al.*, 2007; *Tingay et al.*, 2008; *Istadi et al.*, 2009], concluding that the eruption will last 23-50 years [*Istadi et al.*, 2009; *Davies et al.*, 2011; *Rudolph et al.*, 2011]. Although ground deformation near Lusi has been used previously to characterize the spatial pattern and rate of subsidence [*Abidin et al.*, 2008] and to study the source of the ground deformation during the first year of the eruption [*Fukushima et al.*, 2009], ground deformation has not been used directly to estimate the longevity of the eruption. We find that the rate of ground deformation, and by inference, pressure in the mud source region, is decreasing exponentially and that discharge will decrease to 10% of the present rate in 5 years.

2. Methods

We measured ground deformation near Lusi using multitemporal interferometric analysis [*Shirzaei*, 2012] of 46 L-band synthetic aperture radar images acquired by the ALOS satellite between October 8, 2006 and April 21, 2011. We list the dates of acquisition in Table 1. To generate a time series of the surface deformation field over Lusi, we employ a multiple-master SAR interferometry approach [*Shirzaei*, 2012]. Given 21 and 25 SAR scenes acquired in descending orbit mode (azimuth = 188° and incidence angle ~ 34.3°) from paths 91 and 92, respectively, we generated 400 interferograms. We provide examples of four interferograms in Supplementary Figure 1. The geometrical phase is estimated and subtracted using satellite precise ephemeris data and a reference SRTM digital elevation model of 90 m resolution [*Farr et al.*, 2007; *Franceschetti*, 1999]. To obtain an unambiguous phase observation from modulo 2π phase change measured in each interferogram, we use a model-assisted approach [*Bathke et al.*, 2011] combined with a 2D phase unwrapping operator [*Chen and Zebker*, 2001] and apply it to high quality pixels in the image [*Costantini and Rosen*, 1999]. The algorithm for identifying high quality pixels is based on estimated phase noise [*Shirzaei*, 2012]. Then, each data set is inverted using a linear unbiased estimation approach [*Bjerhammar*, 1973] to generate the time series of the displacement field. We note that through this procedure very localized and rapid deformation components may be lost, but the general trend due to mud source deformation, the subject of this study, is preserved. By applying a temporal high pass and spatial low pass filter we reduce the effect of atmospheric delay on the displacement time series [*Shirzaei*, 2012]. The cumulative displacements during the period of study are shown as contours in Figure 1 and we show the intermediate displacements in Supplementary Figure 2. Time series of displacements at several locations are shown in Supplementary Figure 3.

We performed principal component analysis (PCA) [*Eckart and Young*, 1936; *Jolliffe*, 1986] directly on the displacement time series. We use PCA because we are interested in extracting the dominant temporal behavior from a spatio-temporal dataset and PCA provides us a tool to do this in a way that is optimal in the sense that the first principal component represents a maximal amount of the variance in our data. We represent the displacement time series $\underline{U}$, as an m-x-p matrix of displacements at m points sampled at p time steps. PCA allows us to represent $\underline{U}$ as a sum of spatial modes ($\underline{X}_i$, m-x-1) multiplied by temporal amplitude coefficients ($\underline{\lambda}_i$, 1-x-p):

$$\underline{U} = \sum_{i=1}^{N} \underline{X}_i \underline{\lambda}_i \quad (1)$$

The spatial modes $\underline{X}_i$ are orthonormal and the first principal component maximizes the variance of the displacement data along the axis $\underline{X}_i$. Because our deformation time series covers an area containing both Lusi and a nearby gas well, we divide the data spatially into two regions. We performed PCA separately for the West and East regions, and we calculate the fraction of the variance in each region explained by the first principal component in each region, denoted f_w and f_e. The West and East regions are separated by a straight line whose azimuth and position were determined by maximizing the 2-norm of the fractional variances in the west and east ($\sqrt{f_w^2 + f_e^2}$).

[1]Department of Earth and Planetary Science, University of California, Berkeley, California, USA.

[2]Disaster Prevention Research Institute, Kyoto University, Uji Prefecture, Japan

0094-8276/13/$5.00

3. Results

The spatial modes associated with the first principal components for both West and East regions are shown in Figure 2a. The first principal component for the West region accounts for 90% of the variance in the displacement dataset and in the East region, the first principal component explains 93% of the variance. In Figure 2b-c, we show the temporal amplitude coefficient for the first principal component for the East and West regions. The temporal amplitude coefficient for each region is well-approximated by an exponential function of time of the form $\lambda = a\exp(-t/b) + c$, where t is time. We fit exponential functions of this form to the temporal amplitude coefficient in both East and West regions and recover b-values of 2.1 ± 0.4 and 4.0 ± 1.4 years with R^2 values of 0.98 and 0.97, respectively. Including additional exponential terms did not significantly improve the quality of the fit. The orientation and horizontal position of the line separating the East and West regions affects the recovered b value for the East region by less than 10%, indicating that our results are not contingent upon the precise choice of the boundary between the regions containing the well and Lusi. The higher principal components (Supplementary Figure 4) contain no obvious signal.

4. Discussion

Previous attempts to estimate the longevity of the Lusi eruption have relied significantly upon estimates of mud discharge combined with differing conceptual models for the mechanics of the eruption. The volume of erupted mud was estimated from detailed field surveys of deposit thickness combined with estimates of inundated area based on satellite photographs [*Istadi et al.*, 2009]. Using estimates of mud source thickness and aerial extent derived from seismic reflection profiles and gravity surveys, *Istadi et al.* [2009] obtained a conservative estimate of longevity (23-35 years) by dividing the available volume of mud by the volumetric discharge.

While the longevity estimate of *Istadi et al.* [2009] made no assumptions about the mechanics of the eruption, subsequent estimates have relied upon mechanical models of the eruption [*Davies et al.*, 2011; *Rudolph et al.*, 2011]. By taking the Monte-Carlo approach to explore the influence of unknown model parameters, probabilistic longevity estimates can be generated from such mechanical models. *Davies et al.* [2011] assumed that the eruption is sustained by overpressure in a deep carbonate aquifer. Water ascends from this aquifer and entrains mud at a rate proportional to the water discharge. Using this conceptual model, the 50th percentile longevity estimate is 26 years [*Davies et al.*, 2011]. *Rudolph et al.* [2011] proposed a different conceptual model for the eruption in which the eruption is driven by overpressure in the mud source region and gas exsolution and expansion, and the mud source expands during the eruption as mud is progressively mobilized. Using this conceptual model, *Rudolph et al.* [2011] obtained 50th percentile longevity estimates between 25-50 years using different probability distributions for the unknown model parameters.

Based on the evolution of the temporal amplitude coefficient of the first principal component of the ground deformation (Figure 2), we conclude that the rate of ground deformation is decreasing in time. If the mud is erupting from a chamber with fixed spatial boundaries and elastic surroundings, surface deformation is linearly proportional to the change in pressure within the mud chamber. Under these assumptions, the evolution of the temporal amplitude coefficient can be used directly as a proxy for the evolution of pressure in the mud source, and the exponential decay time scale of the ground deformation (2.1 ± 0.4 years) is the same as the exponential decay time scale of pressure in the mud source region. Because discharge is linearly proportional to the driving pressure gradient when conduit geometry and mud rheology are constant, we can use the exponential decay timescale associated with ground deformation directly as a proxy for the exponential decay timescale of discharge. Discharge from an overpressured mud chamber with elastic surroundings is expected to decrease exponentially, a result that holds true regardless of whether volatile exsolution occurs in the mud source [*Woods and Huppert*, 2003].

Discharge from Lusi was $\sim 10^5$ m^3/day in late 2006 [*Mazzini et al.*, 2007] and has subsequently decreased to $\sim 10^4$ m^3/day [*Mazzini et al.*, 2012]. We plot discharge measurements together with an exponential fit to the discharge measurements of the form $y = a\exp(-t/b)$ in Figure 3. The e-folding time b recovered by fitting the discharge measurements is 1.2 ± 0.8 years. The reported uncertainty should be viewed as a lower bound as the methodology, timing, and uncertainty associated with the discharge measurements are not documented in the literature. Thus, we find that the evolution of the eruption inferred from discharge measurements is consistent with (though less certain than) our geodetic observations. Assuming that the same behavior of the eruption over the last six years continues (e.g. no caldera forms and the mud chamber and conduit geometry do not change), we expect that the discharge at Lusi will decrease by an order of magnitude to $< 10^3$ m^3/day by 2017 ± 1 year.

As the eruption proceeds, elastic stresses generated in response to the withdrawal of mud from depth will continue to increase, and these stresses could still become sufficiently large to mobilize additional mud [*Rudolph et al.*, 2011] or to cause a caldera to form. If a caldera forms, pressure in the mud source region is no longer expected to decrease exponentially in time. Rather, pressure will be buffered by the overburden of the caldera's lid, which will be coupled to its surroundings by friction on Caldera-bounding faults. If there is an external fluid reservoir involved in the eruption [*Davies et al.*, 2011; *Mazzini et al.*, 2012], our longevity assessment is unaffected because the surface deformations result from withdrawal of mud that becomes entrained in the erupting water, and the entrainment rate is related to the discharge from (and overpressure in) the hypothetical external fluid reservoir, in which pressure is expected to decrease exponentially in time.

Acknowledgments. This work was supported in part by funding from the National Science Foundation.

References

Abidin, H. Z., R. Davies, M. Kusuma, H. Andreas, and T. Deguchi, Subsidence and uplift of Sidoarjo (East Java) due to the eruption of the Lusi mud volcano (2006-present), *Environmental Geology*, 2008.

Bathke, H., M. Shirzaei, and T. R. Walter, Inflation and deflation at the steep-sided Llaima stratovolcano (Chile) detected by using InSAR, *Geophys. Res. Lett*, *38*(10), L10,304, 2011.

Bjerhammar, A., *Bjerhammar (1973) Theory of errors and generalized matrix inverses*, Elsevier, Amsterdam, 1973.

Chen, C. W., and H. A. Zebker, Two-dimensional phase unwrapping with use of statistical models for cost functions in nonlinear optimization, *Journal of the Optical Society of America A: Optics*, *18*(2), 338–351, 2001.

Costantini, M., and P. A. Rosen, A generalized phase unwrapping approach for sparse data, in *Proceedings IEEE 1999 International Geoscience and Remote Sensing Symposium*, pp. 267–269, IEEE, 1999.

Davies, R. J., S. Mathias, R. E. Swarbrick, and M. Tingay, Probabilistic longevity estimate for the LUSI mud volcano, East Java, *Journal of the Geological Society*, *168*(2), 517–523, 2011.

Eckart, C., and G. Young, The approximation of one matrix by another of lower rank, *Psychometrika*, *1*(3), 211–218, 1936.

Farr, T. G., P. A. Rosen, E. Caro, R. Crippen, R. Duren, S. Hensley, M. Kobrick, M. Paller, E. Rodriguez, L. Roth, D. Seal, S. Shaffer, J. Shimada, J. Umland, M. Werner, M. Oskin, D. Burbank, and D. Alsdorf, The Shuttle Radar Topography Mission, *Rev. Geophys.*, *45*(2), 2007.

Franceschetti, G., *Synthetic aperture radar processing*, CRC Press, Boca Raton, 1999.

Fukushima, Y., J. Mori, M. Hashimoto, and Y. Kano, Subsidence associated with the LUSI mud eruption, East Java, investigated by SAR interferometry, *Marine and Petroleum Geology*, *26*(9), 1740–1750, 2009.

Istadi, B., G. Pramono, and P. Sumintadireja, Modeling study of growth and potential geohazard for LUSI mud volcano: East Java, Indonesia, *Marine and Petroleum Geology*, *26*, 1724–1739, 2009.

Jolliffe, I., *Principal Component Analysis*, Springer-Verlag, 1986.

Mazzini, A., H. Svensen, G. Akhmanov, G. Aloisi, S. Planke, A. Malthe-Sørenssen, and B. Istadi, Triggering and dynamic evolution of Lusi mud volcano, Indonesia, *Earth and Planetary Science Letters*, *261*, 375–388, 2007.

Mazzini, A., A. Nermoen, M. Krotkiewski, Y. Podladchikov, S. Planke, and H. Svensen, Strike-slip faulting as a trigger mechanism for overpressure release through piercement structures. Implications for the Lusi mud volcano, Indonesia, *Marine and Petroleum Geology*, *26*(9), 1751–1765, 2009.

Mazzini, A., G. Etiope, and H. Svensen, A new hydrothermal scenario for the 2006 Lusi eruption, Indonesia. Insights from gas geochemistry, *Earth and Planetary Science Letters*, *317–318*(0), 305–318, 2012.

Richards, J. R., Report into the Past, Present, and Future Social Impacts of Lumpur Sidoarjo, *Tech. rep.*, Humanitus Sidoarjo Fund, 2011.

Rudolph, M. L., L. Karlstrom, and M. Manga, A prediction of the longevity of the Lusi mud eruption, Indonesia, *Earth and Planetary Science Letters*, *308*(1-2), 124–130, 2011.

Shirzaei, M., A Wavelet-Based Multitemporal DInSAR Algorithm for Monitoring Ground Surface Motion, *IEEE Geoscience and Remote Sensing Letters*, *PP*(99), 1–5, 2012.

Tingay, M., O. Heidbach, R. Davies, and R. Swarbrick, Triggering of the Lusi mud eruption: Earthquake versus drilling initiation, *Geology*, *36*(8), 639–642, 2008.

Woods, A. W., and H. E. Huppert, On magma chamber evolution during slow effusive eruptions, *J. Geophys. Res.*, *108*(B8), 2403, 2003.

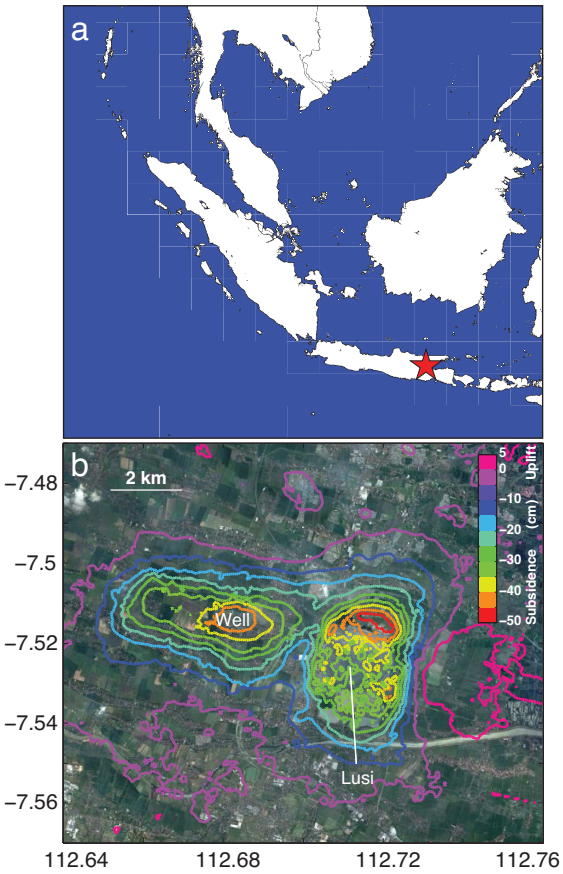

Figure 1. (a) Regional map showing Lusi's location (indicated by red star) in East Java. (b) Contour plot of cumulative vertical displacement showing subsidence due to Lusi and a nearby well between October, 2006 and April, 2011 superimposed on a satellite photo of the affected area.

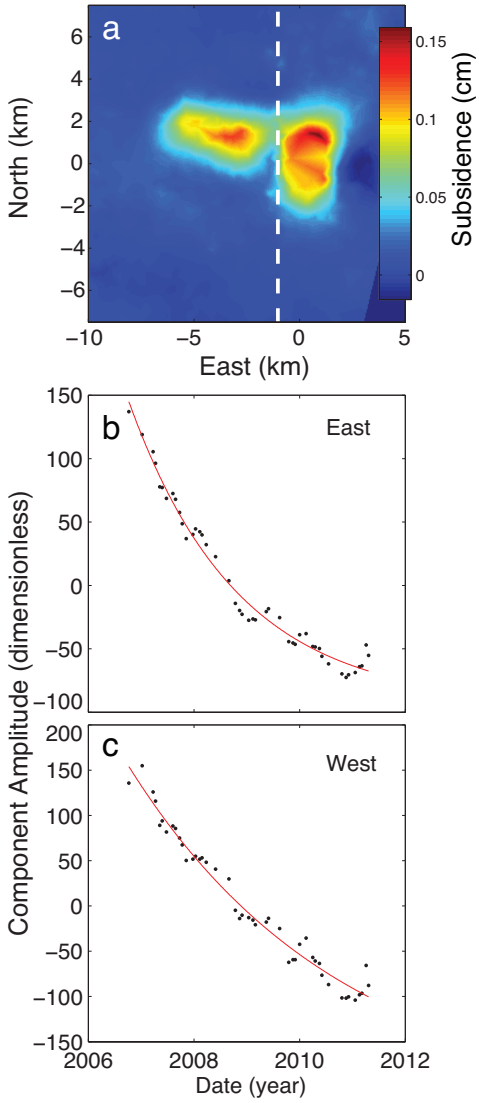

Figure 2. Results of principle component analysis of ground deformation data. (a) Spatial pattern associated with first principal component. Data has been projected onto a regular grid for visualization. White dashed line indicates boundary between West (well) and East (Lusi) regions. (b) Temporal weighting coefficient (black) and a best fit exponential curve (red) for East region. (c) same as (b) for West region. Both positive and negative values are expected because the deformation described by PCA is measured relative to the temporal mean displacement.

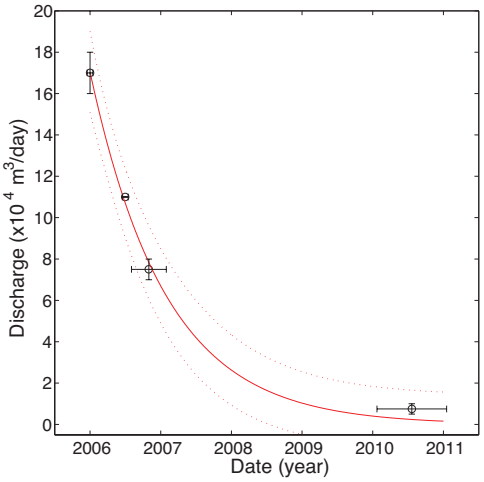

Figure 3. Discharge measured at Lusi from December 2006 onwards [*Mazzini et al.*, 2007, 2009, 2012]. Vertical bars indicate the range of reported values. The precise date on which discharge measurements were made are not always reported and horizontal bars indicate the approximate time period in which each discharge measurement was made. The red solid line is the best fit to the discharge measurements and the dashed lines show the 95% confidence interval for this fit.

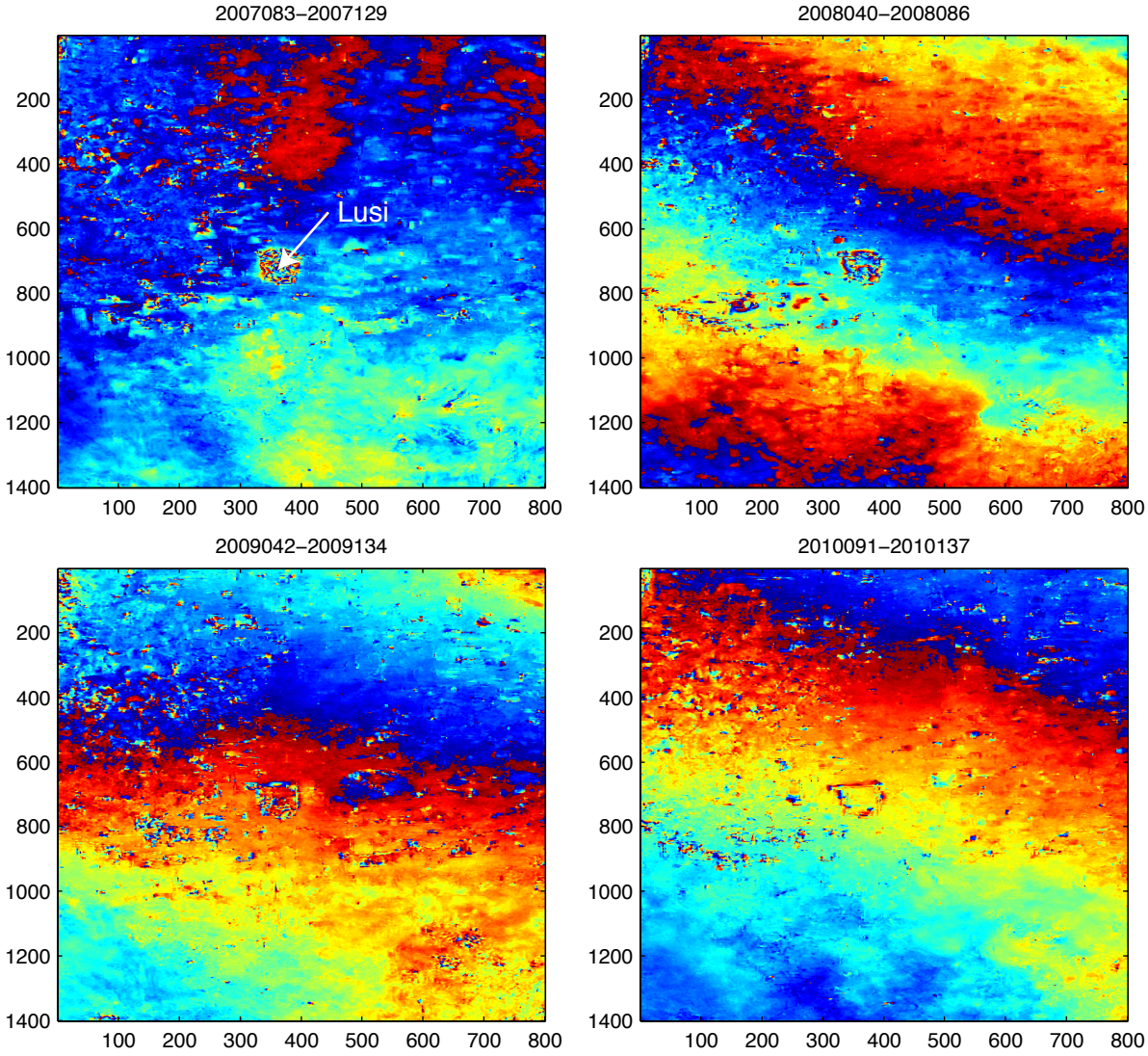

Supplementary Figure 1: Four interferograms, each spanning 46 days (except for lower left - 92 days). Interferograms are shown in the radar coordinate system, with pixel size approximately 40x40 m. No filtering has been applied, and orbital ramps have not been corrected. The radar wavelength is 23.6 cm.

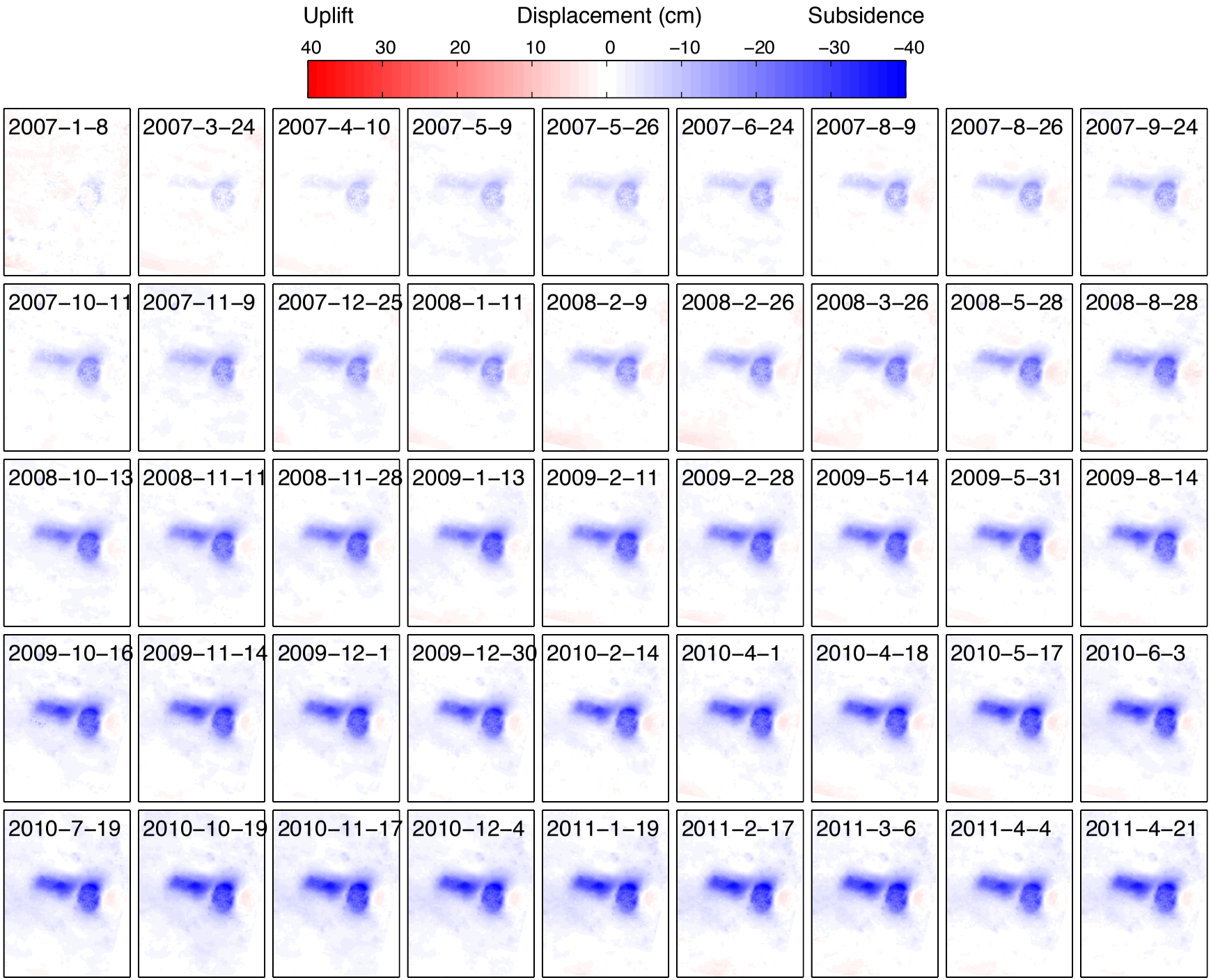

Supplementary Figure 2: Cumulative vertical ground displacement since October 8, 2006.

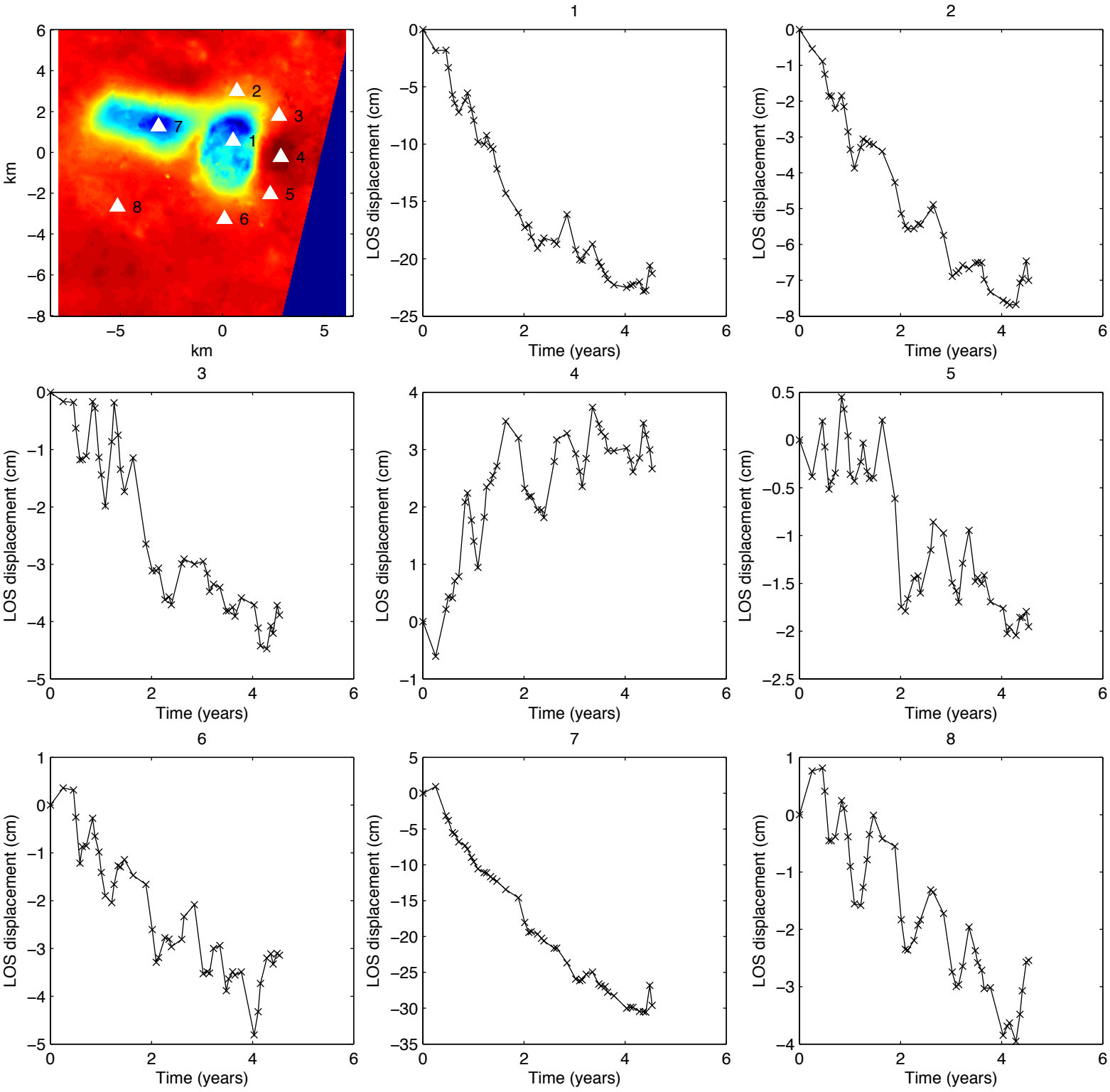

Supplementray Figure 3: (top left) Cumulative vertical line-of-sight (LOS) displacements between October 2006 and April 2011. Other panels show displacement time series at locations indicated by numbered triangles in top left panel.

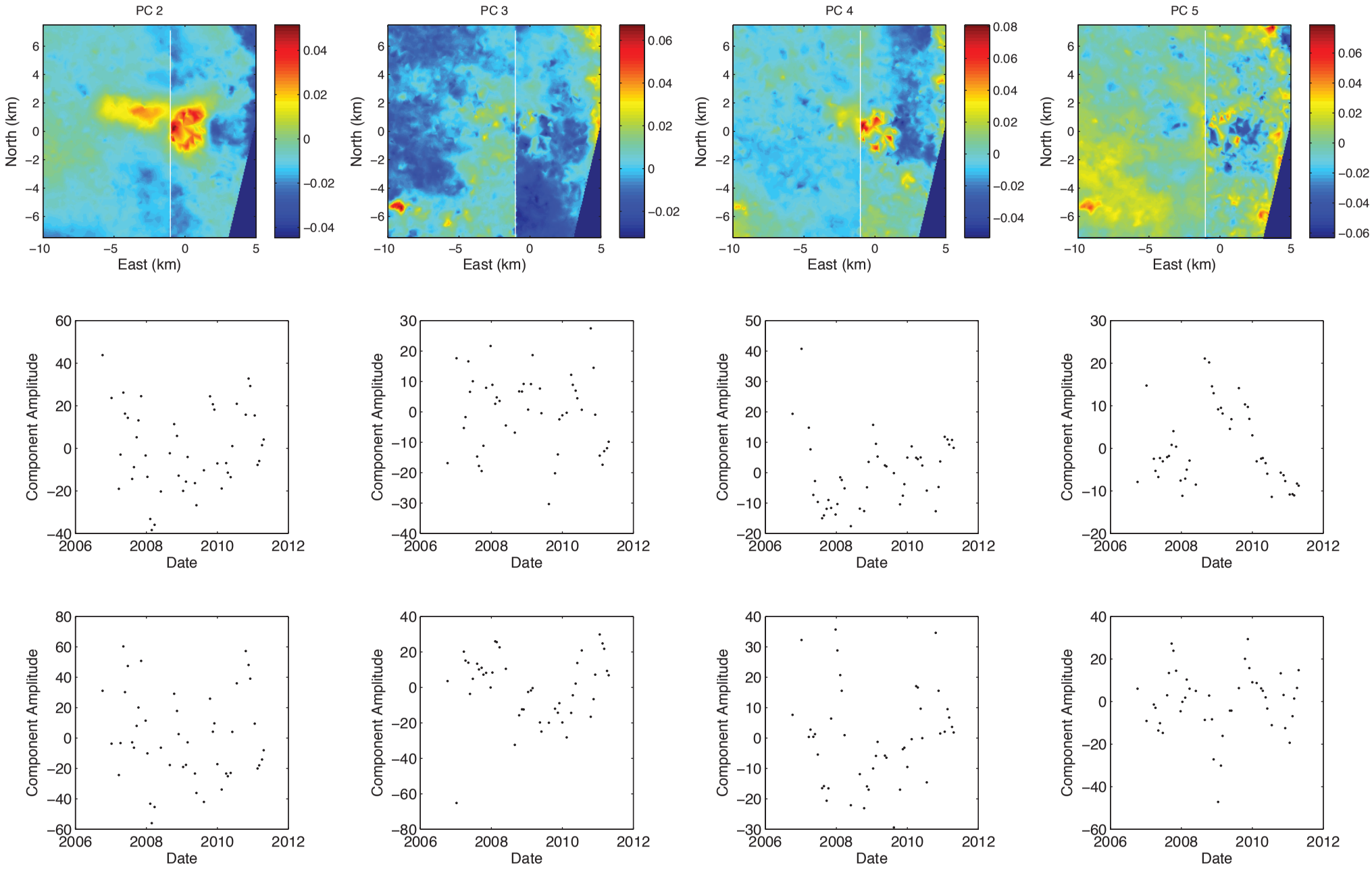

Supplementary Figure 4: Spatial patterns (top) and temporal coefficients for the 2nd through 5th principal components for the East (middle) and West (bottom) regions.